Hdac4 mediates perichondral ossification and pharyngeal skeleton development in the zebrafish (#29625)

First submission

Editor guidance

Please submit by 13 Aug 2018 for the benefit of the authors (and your \$200 publishing discount).



Structure and Criteria

Please read the 'Structure and Criteria' page for general guidance.



Custom checks

Make sure you include the custom checks shown below, in your review.



Author notes

Have you read the author notes on the guidance page?



Raw data check

Review the raw data. Download from the materials page.



Image check

Check that figures and images have not been inappropriately manipulated.

Privacy reminder: If uploading an annotated PDF, remove identifiable information to remain anonymous.

Files

Download and review all files from the <u>materials page</u>.

Custom checks

6 Figure file(s)

2 Table file(s)

Vertebrate animal usage checks

- Have you checked the authors ethical approval statement?
- Were the experiments necessary and ethical?
- Have you checked our <u>animal research policies</u>?

Structure your review

The review form is divided into 5 sections. Please consider these when composing your review:

- 1. BASIC REPORTING
- 2. EXPERIMENTAL DESIGN
- 3. VALIDITY OF THE FINDINGS
- 4. General comments
- 5. Confidential notes to the editor
- You can also annotate this PDF and upload it as part of your review

When ready submit online.

Editorial Criteria

Use these criteria points to structure your review. The full detailed editorial criteria is on your guidance page.

BASIC REPORTING

- Clear, unambiguous, professional English language used throughout.
- Intro & background to show context. Literature well referenced & relevant.
- Structure conforms to Peerl standards, discipline norm, or improved for clarity.
- Figures are relevant, high quality, well labelled & described.
- Raw data supplied (see Peerl policy).

EXPERIMENTAL DESIGN

- Original primary research within Scope of the journal.
- Research question well defined, relevant & meaningful. It is stated how the research fills an identified knowledge gap.
- Rigorous investigation performed to a high technical & ethical standard.
- Methods described with sufficient detail & information to replicate.

VALIDITY OF THE FINDINGS

- Impact and novelty not assessed. Negative/inconclusive results accepted. Meaningful replication encouraged where rationale & benefit to literature is clearly stated.
- Data is robust, statistically sound, & controlled.
- Speculation is welcome, but should be identified as such.
- Conclusions are well stated, linked to original research question & limited to supporting results.

Standout reviewing tips



The best reviewers use these techniques

	p

Support criticisms with evidence from the text or from other sources

Give specific suggestions on how to improve the manuscript

Comment on language and grammar issues

Organize by importance of the issues, and number your points

Please provide constructive criticism, and avoid personal opinions

Comment on strengths (as well as weaknesses) of the manuscript

Example

Smith et al (J of Methodology, 2005, V3, pp 123) have shown that the analysis you use in Lines 241-250 is not the most appropriate for this situation. Please explain why you used this method.

Your introduction needs more detail. I suggest that you improve the description at lines 57-86 to provide more justification for your study (specifically, you should expand upon the knowledge gap being filled).

The English language should be improved to ensure that an international audience can clearly understand your text. Some examples where the language could be improved include lines 23, 77, 121, 128 - the current phrasing makes comprehension difficult.

- 1. Your most important issue
- 2. The next most important item
- 3. ...
- 4. The least important points

I thank you for providing the raw data, however your supplemental files need more descriptive metadata identifiers to be useful to future readers. Although your results are compelling, the data analysis should be improved in the following ways: AA, BB, CC

I commend the authors for their extensive data set, compiled over many years of detailed fieldwork. In addition, the manuscript is clearly written in professional, unambiguous language. If there is a weakness, it is in the statistical analysis (as I have noted above) which should be improved upon before Acceptance.



Hdac4 mediates perichondral ossification and pharyngeal skeleton development in the zebrafish

April DeLaurier Corresp., Cynthia Lizzet Alvarez 1, Kali J Wiggins 1

Corresponding Author: April DeLaurier Email address: aprild@usca.edu

Background. Histone deacetylases (Hdacs) are epigenetic factors that function to repress gene transcription by removing acetyl groups from the N-terminal of histone lysines. Histone deacetylase 4 (HDAC4), a class IIa HDAC, has previously been shown to regulate the process of endochondral ossification in mice via repression of Myocyte enhancing factor 2c (MEF2C), a transcriptional activator of Runx2, which in turn promotes chondrocyte maturation and production of bone by osteoblasts.

Methods & Materials. In this study we generated two zebrafish lines with mutations in *hdac4* using CRISPR/Cas9 and analyzed mutants for skeletal phenotypes and expression of genes known to be affected by Hdac4/Mef2c interactions

Results: Lines have insertions causing a frameshift in a proximal exon of *hdac4* and a premature stop codon. Mutations are predicted to result in aberrant protein sequence and a truncated protein, eliminating the Mef2c binding domain and Hdac domain. Zygotic mutants show a mild to moderate increase in ossification of pharyngeal ceratohyal and to some extent hyosymplectic cartilages at 7 days post fertilization (dpf). mRNA *in situ* hybridization at 72 hpf shows that *hdac4* is normally expressed in regions of the wild-type ceratohyal, hyosymplectic, and posterior pharyngeal arch cartilages, indicating that loss of function may lead to premature or excessive ossification at these sites. At 4 dpf, mutant larvae have an increase of expression of *runx2a* and *sp7* in the ceratohyal cartilage, which we hypothesize is due to the de-repression of Mef2c through loss of Hdac4. Expression of *runx2b* was unchanged in mutants compared to wild types. A subset of maternal-zygotic mutant and heterozygote larvae show a dramatically increased level of ossification at 7 dpf compared to zygotic mutants, including formation of a precocious anguloarticular bone and mineralization of the ceratobranchial and symplectic cartilages, which normally does not occur until fish are approximately 12 dpf. Some maternal-zygotic mutants and heterozygotes also show loss of pharyngeal first arch elements, suggesting loss of Hdac4 may affect neural crest development.

Discussion. The results of this study demonstrate a role for Hdac4 in zebrafish cartilage ossification consistent with the function of this protein in mice, indicating that the function of Hdac4 in skeletal development is conserved among vertebrates. Furthermore, we have identified a potentially novel role for maternal Hdac4 in zebrafish cartilage ossification and neural crest development.

¹ Department of Biology and Geology, University of South Carolina - Aiken, Aiken, South Carolina, United States



Hdac4 mediates perichondral ossification and pharyngeal skeleton development in the zebrafish

pharyngeai skeleton development in the zebralish
April DeLaurier ¹ , Cynthia Lizzet Alvarez ¹ , Kali J Wiggins ¹
¹ Department of Biology and Geology, University of South Carolina Aiken, Aiken, South Carolina, USA
Corresponding Author: April DeLaurier ¹
Dept. of Biology and Geology, University of South Carolina Aiken, 471 University Parkway Aiken, South Carolina, 29801, USA
Email address: aprild@usca.edu



19 Abstract

20 Background. Histone deacetylases (Hdacs) are epigenetic factors that function to 21 repress gene transcription by removing acetyl groups from the N-terminal of histone 22 lysines. Histone deacetylase 4 (HDAC4), a class IIa HDAC, has previously been shown 23 to regulate the process of endochondral ossification in mice via repression of Myocyte enhancing factor 2c (MEF2C), a transcriptional activator of Runx2, which in turn 24 25 promotes chondrocyte maturation and production of bone by osteoblasts. 26 **Methods & Materials.** In this study, we generated two zebrafish lines with mutations in 27 hdac4 using CRISPR/Cas9 and analyzed mutants for skeletal phenotypes and 28 expression of genes known to be affected by Hdac4/Mef2c interactions. 29 **Results:** Lines have insertions causing a frameshift in a proximal exon of *hdac4* and a 30 premature stop codon. Mutations are predicted to result in aberrant protein sequence 31 and a truncated protein, eliminating the Mef2c binding domain and Hdac domain. 32 Zygotic mutants show a mild to moderate increase in ossification of pharyngeal 33 ceratohyal and to some extent hyosymplectic cartilages at 7 days post fertilization (dpf). 34 mRNA in situ hybridization at 72 hpf shows that hdac4 is normally expressed in regions 35 of the wild-type ceratohyal, hyosymplectic, and posterior pharyngeal arch cartilages, 36 indicating that loss of function may lead to premature or excessive ossification at these 37 sites. At 4 dpf, mutant larvae have an increase of expression of runx2a and sp7 in the 38 ceratohyal cartilage, which we hypothesize is due to the de-repression of Mef2c through 39 loss of Hdac4. Expression of runx2b was unchanged in mutants compared to wild types. 40 A subset of maternal-zygotic mutant and heterozygote larvae show a dramatically 41 increased level of ossification at 7 dpf compared to zygotic mutants, including formation



42 of a precocious anguloarticular bone and mineralization of the ceratobranchial and 43 symplectic cartilages, which normally does not occur until fish are approximately 12 dpf. 44 Some maternal-zygotic mutants and heterozygotes also show loss of pharyngeal first 45 arch elements and neurocranium defects, suggesting loss of Hdac4 may affect neural 46 crest development. 47 **Discussion.** The results of this study demonstrate a role for Hdac4 in zebrafish 48 cartilage ossification consistent with the function of this protein in mice, indicating that 49 the function of Hdac4 in skeletal development is conserved among vertebrates. 50 Furthermore, we have identified a potential role for maternal Hdac4 in zebrafish 51 cartilage ossification and neural crest development. 52 53 Introduction 54 The majority of the vertebrate skeleton including the axial, limb, and pharyngeal 55 elements form as cartilaginous elements that grow rapidly during early development 56 through the proliferation of matrix-secreting chondrocytes. At specific stages of 57 development, chondrocytes cease their rapid proliferation and matrix secretion, become 58 hypertrophic, and signal to nearby cells to commence endochondral ossification 59 (Karsenty & Wagner, 2002). In zebrafish, ossification involves the recruitment of 60 osteoblasts to the surface of cartilage to secrete a perichondral collar of mineralized 61 bone. In amniotes, endochondral ossification involves both perichondral ossification and 62 the invasion of the cartilage by blood vessels to deliver osteoblasts which deposit bone 63 (Hall, 2014). In all vertebrates, the timing of the transition between endochondral growth 64 and ossification is important in the determining size and shape of skeletal elements.



65 This process is precisely regulated by expression of factors in chondrocytes and 66 osteoblasts including Ihh, Pthrp, Runx2 (Cbfa1), and Sp7 (osterix) (Vortkamp et al., 67 1996; Komori et al., 1997; Nakashima et al., 2002; Maeda et al., 2007). Loss of function 68 of these factors can cause insufficient ossification, resulting in severe growth and 69 patterning defects of the skeleton (Quack et al., 1999; Wysolmerski et al., 2001; Gao et 70 al., 2001; Valadares et al., 2014). 71 Histone deacetylase 4 (HDAC4), a member of the class IIa group of HDACs 72 (including HDAC 4, 5, 7, and 9), has previously been demonstrated to be an important 73 regulator of chondrocyte maturation and initiation of endochondral ossification in mice 74 (Vega et al., 2004). HDACs lack the ability to bind to DNA directly, but associate with 75 other proteins to remove acetyl groups from the N-terminal of histone lysines, causing 76 histones to condense, blocking access of transcription factors to DNA, resulting in 77 transcriptional repression (Haberland, Montgomery & Olson, 2009). Class IIa HDACs 78 are characterized by a carboxyl-terminal binding protein domain (CtBP), a MEF2 79 binding domain for binding the transcription factor myocyte enhancing factor 2c 80 (MEF2C), sites for binding of the chaperone protein 14-3-3, and an HDAC domain 81 (Haberland, Montgomery & Olson, 2009). MEF2C is a transcription factor which controls 82 chondrocyte hypertrophy and bone formation by activating transcription of target genes 83 such as Runx2 (Arnold et al., 2007). When class IIa HDACs are unphosphorylated, they 84 localize to the nucleus where they bind to MEF2C, and function to repress transcription 85 of MEF2C-target genes (Lu et al., 2000; Passier et al., 2000; McKinsey et al., 2000; 86 Arnold et al., 2007). When calcium/calmodulin protein kinase (CaMKII) and protein 87 kinase D (PKD) phosphorylate 14-3-3 and shuttle the HDAC into the cytoplasm, MEF2C



98

99

100

101

102

103

104

105

106

107

108

109

110

88 becomes unbound to HDAC, and can activate transcription of target genes (Lu et al., 89 2000; Passier et al., 2000; McKinsey et al., 2000). Through this process of interaction 90 with MEF2C, HDAC4 delays the hypertrophy of chondrocytes within cartilage, 91 controlling the timing and extent of ossification of endochondral bone by osteoblasts 92 (Vega et al., 2004). 93 Zebrafish represent a useful model for studying mechanisms of chondrocyte 94 maturation and the initiation of the cartilage ossification process as they develop 95 cartilaginous elements as early as 60-72 hours post-fertilization and commence

97 Compared with other vertebrates, zebrafish undergo the same cellular and genetic

perichondral ossification of these elements as early as 96 hpf (Eames et al., 2013).

signaling pathways associated with skeletal ossification including chondrocyte

hypertrophy, differentiation and matrix secretion by osteoblasts, including expression of

factors associated with ossification such as ihha, runx2a, runx2b, sp7, col1a2, col10a1,

and osteonectin (Flores et al., 2004; Avaron et al., 2006; Li et al., 2009). These

similarities make zebrafish a useful model to study genetic pathways associated with

skeletal development and disease.

In this study, we describe two zebrafish lines with early frameshift mutations in *hdac4*. Mutant larvae from heterozygote in-crosses show a mild_to moderate increase in ossification of certain pharyngeal cartilage elements, and an up-regulation of markers of ossification of the skeleton including *runx2a* and *sp7*. A further enhancement of the excessive ossification defect is observed in maternal-zygotic mutants, indicating an early maternal contribution to regulation of skeletal patterning in zebrafish. Previously, we identified a potential role for Hdac4 in neural crest development and neurocranium



formation in zebrafish (DeLaurier et al., 2012). Although this phenotype was not reproduced in any zygotic mutants, a profound loss of anterior facial structures was observed in a subset of maternal-zygotic mutants, indicating a function for maternal Hdac4 in neural crest development or formation of other anterior structures of the head or face. In conclusion, *hdac4* mutants reproduce aspects of the mouse HDAC4 mutant and may be a useful model, especially along with other reverse-genetic mutants for other class Ila Hdacs, to study the function of these factors in skeletal patterning and other developmental pathways.

Methods

Zebrafish husbandry

AB strain wild-type (WT) zebrafish were originally obtained from the Zebrafish International Resource Center (ZIRC, Eugene, OR). Fish were reared and maintained at 28.5°C on a 14 hour on/10 hour off light cycle. Fish were fed as previously described (Wasden, Roberts & DeLaurier, 2017). Maintenance and use of zebrafish followed guidelines from ZIRC, the Zebrafish book (Westerfield, 2007), and the Institutional Animal Care and Use Committee (IACUC) of the University of South Carolina Aiken (approval number 010317-BIO-01).

Generation of CRISPR lines

The CRISPR/Cas9 procedure was based on previously described methodologies

(Hwang et al., 2013). CHOPCHOP (http://chopchop.cbu.uib.no/) was used to design a



134	guide RNA (gRNA) sequence targeting exon 5 of <i>hdac4</i> (ensembl
135	ENSDART00000165238.3), 5' of the Mef2c binding site (located in exon 6) and histone
136	deacetylase domain, with minimal potential off-target binding (Montague et al., 2014;
137	Labun et al., 2016). An <i>hdac4</i> -specific oligonucleotide was designed containing a 20 bp
138	T7 promoter sequence, 20bp of target sequence (GGAGCGTCATCGACAGGAGC),
139	followed by a 20 bp scaffold overlap sequence as described (Bassett et al., 2013). This
140	oligonucleotide was annealed to a scaffold oligonucleotide containing the tracrRNA
141	stem loop sequence using Phusion PCR (New England Biolabs, Ipswich, MA) to
142	produce a 120 bp template. Template DNA was column purified (DNA Clean &
143	Concentrator kit, Zymo Research, Irvine, CA) and was used to synthesize RNA using
144	T7 polymerase (MAXIscript T7 Transcription kit, Thermo Fisher, Vitnus, Lithuania).
145	Cas9 mRNA was synthesized from pCS2-nCas9n (Addgene, Cambridge, MA). Plasmid
146	was linearized with Notl-HF (New England Biolabs, Ipswich, MA), column purified
147	(Zyppy Plasmid Miniprep kit, Zymo Research, Irvine, CA), and mRNA was synthesized
148	(mMessenger mMachine SP6 kit, Thermo Fisher, Vitnus, Lithuania). Column-purified
149	hdac4 gRNA and nCas9n mRNA (RNA Clean & Concentrator kit, Zymo Research,
150	Irvine, CA) were co-injected into one cell-stage embryos. Each embryo was injected
151	with approximately 3nl of a 5ul mix containing <i>hdac4</i> gRNA (~60ng/microliter), nCas9n
152	mRNA (~160ng/microliter), and phenol red as a marker. Unfertilized or dead embryos
153	were removed from the dish at the end of the first day of injection and on subsequent
154	days.

156

Identification of founders and generation of mutant lines



157	At 36 hpf, approximately 20% of injected embryos (abnormal and normal-looking) were
158	pooled into groups of 5 fish per tube, lysed using HotShot (Truett et al., 2000), and PCR
159	was performed using genomic primers flanking the site of potential mutation. PCR
160	products were gel-purified and digested using T7 endonuclease (New England Biolabs,
161	Ipswich, MA) to identify mismatched DNA indicating potential founder lines (Hwang et
162	al., 2013). Siblings of fish (approximately 40 fish) with positive T7 results were reared to
163	adulthood and used as founder (F_0) lines for subsequent experiments. Three F_0 fish
164	demonstrated germ line transmission to offspring, and F ₁ lines were generated from
165	these founders by out-crossing founders to AB wild types. Adult F_1 fish were identified
166	as heterozygous carriers of potential mutations using PCR and T7 endonuclease digest
167	on fin clip DNA. Heterozygous F_1 fish were outcrossed to generate F_2 lines, and F_2 lines
168	were in-crossed to produce homozygous mutants. PCR products from potential mutants
169	and wild type siblings were sequenced (Eurofins, Louisville, KY) and genomic
170	sequences were compared to wild-type siblings to identify mutations (Geneious, version
171	8, http://www.geneious.com) (Kearse et al., 2012). Mutations were confirmed by RT-
172	PCR of cDNA (RevertAid First Strand cDNA Synthesis kit, Thermo Fisher, Vitnus,
173	Lithuania) using an exon 3 forward primer 5'-gccactggaacttctcaagc-3' and an exon 6
174	reverse primer 5'-gcagtggttgagactcctct-3' (Tm = 58°C x40 cycles or Touchdown PCR,
175	Tm = $72-65^{\circ}$ C x15 cycles followed by Tm = 64.5° C x20 cycles). RT-PCR products were
176	column purified as described above and sequenced to confirm the mutation.
177	Heterozygous F_2 and F_3 carriers of mutant alleles were in-crossed to produce wild type,
178	heterozygote, and mutant offspring. Maternal-zygotic mutants were generated by
179	crossing a homozygote mutant female with a heterozygote male.



Genotyping adults and larvae

Fin clips from adult fish and fin clips or whole larvae used for histological stains were genotyped using Hotshot lysis as described above. An 822bp region of exon 5 spanning the site of mutation in *hdac4* was PCR-amplified using an intron 4-5 forward primer 5'-atgttctccctgtgttggtg-3' and an intron 5-6 reverse primer 5'-gctgtatttccgctcatgtg-3' (Tm = 58°C, x40 cycles). PCR products were run on a 2% agarose gel at 60V for 5-6 hours to produce band separation sufficient to distinguish heterozygote (2 bands) fish from wild type and mutant fish (both 1 lower and upper band, respectively).

Histological stains and mRNA in situ hybridization

Alcian Blue and Alizarin Red staining to label cartilage and bone was performed as described (Walker & Kimmel, 2007). Double fluorescent mRNA *in situ* hybridization was performed as described (Talbot, Johnson & Kimmel, 2010), using probes for *hdac4*, *runx2a*, *runx2b*, *sp7*, and *sox9a* (DeLaurier et al., 2010; Huycke, Eames & Kimmel, 2012). For each mRNA *in situ* hybridization experiment, 5-10 individual wild type and mutant larvae were imaged and analyzed. Representative examples of expression patterns are shown in this paper.

Imaging and image analysis and statistics

Alcian Blue and Alizarin Red stained specimens were dissected and flat mounted on microscope slides and imaged on a compound microscope. The right pharyngeal skeleton was flat mounted for each specimen unless it was damaged or defective, in



204

205

206

207

208

209

210

which case the left side was used. The areas of flat mounted ceratohyal and hyomandibula cartilages were measured using pixel area of cartilage and bone using ImageJ (NIH). The area of bone as a ratio of cartilage area was used a measure of ossification in statistical analysis. In total, 93 fish were measured for the *aik2* line (wild type = 38, heterozygote = 23, mutant = 32) and 61 fish were measured for the *aik3* line (wild type = 17, heterozygote = 28, mutant = 16). Statistical analyses were performed in SAS 9.4 (SAS Institute, Carey, NC). Fluorescent confocal microscopy was performed using a Leica SPEII confocal microscope (Leica Microsystems, Buffalo Grove, IL).

211

212

Results

213

214

Hdac4 mutants have a frameshift lesion

215 Using CRISPR/Cas9 to target exon 5 of hdac4 (Fig. 1A), we induced frameshift 216 mutations in two individual fish that were used to generate mutant lines. Line 217 hdac4aik2/aik2 has a 19 bp insertion three bases upstream of the protospacer adjacent 218 motif (PAM) site associated with Cas9 binding and cleaving of DNA. Line hdac4aik3/aik3 219 has a 2 bp insertion, followed by retention of 7 bp of the wild-type sequence, followed by 220 a 27 bp insertion one base pair upstream of the PAM site (Fig. 1B). In both cases, 221 frameshifts were induced by insertion of nucleotides into exon 5, resulting in aberrant 222 amino acids being added to the protein sequence (Fig. 1C). In both mutant lines the 223 frameshift is predicted to cause the loss of the Mef2c binding domain and premature 224 stop codons resulting in truncated proteins 174 aa (hdac4aik2/aik2) and 181 aa 225 (hdac4aik3/aik3) in length (Fig. 1D). Frameshifts were detected in mutant cDNA compared



227

228

229

230

231

232

233

234

235

236

237

238

239

240

to wild type cDNA using primers spanning exons 3-6, and there was no evidence of splice variants or exon skipping detected on agarose gels for either mutant (Figs. 1E and F). In the case of *hdac4*^{aik3/aik3}, a larger band was detected along with the band of expected size (Fig. 1F, indicated by asterisk). This band was excised and sequenced and was found to have an identical sequence to the band of the expected size. We interpret that this larger band is the product of heterodimers of our PCR product or a slower running single-stranded DNA product and not a splice variant or other genomic feature within the mutant. In both the hdac4aik2/aik2 and hdac4aik3/aik3 lines, adult fish and embryos were genotyped using intronic primers spanning exon 5. The larger mutant band (841 bp hdac4aik2/aik2, 858 bp hdac4aik3/aik3) can be distinguished from the wild type band (822bp), and heterozygotes show both bands (Figs. 1G and H). At 7dpf and earlier, mutant embryonic and larval fish have no discernable abnormalities compared to wild type siblings (Figs. 1I and J). Mutant fish form swim bladders, feed, and grow normally into adult fish. Mutant fish from the hdac4aik2/aik2 line also showed no overt abnormalities compared to wild type siblings (data not shown).

241

242

243

244

245

246

247

248

Mutants have increased ossification of pharyngeal cartilage

Heterozygous in-crosses were used to generate wild type, heterozygous, and mutant larvae for skeletal preparations and analysis. At 7 dpf, mutants from the *aik2* and *aik3* lines showed a greater extent of ossification of the ceratohyal cartilage compared to wild-type siblings (Fig. 2B-F, *aik2* only shown in D-F, *aik3* not shown). Wild type fish typically had a small area of bone stain localized to the mid-shaft of the ceratohyal, usually appearing first at the dorsal margin of the cartilage and spreading ventrally (Fig.



250

251

252

253

254

255

256

257

258

259

260

261

262

263

264

265

266

267

268

269

270

271

2D and D'). Among mutants, excess bone was observed at the mid-shaft of the ceratohyal, either as a mild (Fig. 2E and E') or moderate (Fig. 2F and F') increase compared to wild types. In mutants, the extent of bone growth appeared to have irregular boundaries compared to the wild type pattern (Fig. 2E indicated by arrow in E') and a greater extent of formation of a perichondral bone collar around the shaft of the ceratohyal (Figs. 2E', F', indicated by asterisks). No other defects were detected in the pharyngeal skeleton in mutants analyzed at this stage. For both the ceratohyal and hyosymplectic, the area of bone and the area of cartilage were measured, and the amount of ossification was calculated as the ratio of bone to cartilage present (Figs. 2G-J). For the aik2 line, ANCOVA revealed that the effect of genotype on the area of ossification of the ceratohyal was significant (F=4.01; df=2,89; p=0.0215). Tukey's multiple comparisons showed that mutants had significantly more bone than wild types (p=0.0057), but heterozygotes were not significantly different from either mutants (p=0.1751) or wild types (p=0.2488) (Fig. 2G). For the aik3 line, ANOVA revealed that the effect of genotype on the area of ossification of the ceratohyal was also significant (F=7.77; df=2,58; p=0.001). Tukey's multiple comparisons showed that mutants had significantly more bone than wild types (p=0.0002), that heterozygotes also had significantly more bone than wild types (p=0.0134), and that there was no significant difference between heterozygotes and mutants (p=0.0697) (Fig. 2H). For the aik2 line, ANOVA revealed no significant effect of genotype on area of ossification of the hyosymplectic (F=2.3; df=2,90; p=10.62) (Fig. 21). For the aik3 line, ANCOVA also revealed no significant effect of genotype on area of

ossification of the hyosymplectic (F=2.48; df=1,56; p=0.0928) (Fig. 2J).

$\overline{}$	$\overline{}$	$\overline{}$
٠,	٠,	٠,
/.	•	/.

hdac4 is expressed in regions of the pharyngeal skeleton consistent with a role in
 cartilage maturation
 At 60 hpf, hdac4 expression is broadly expressed throughout the head, with no

At 60 hpf, hdac4 expression is broadly expressed throughout the head, with no apparent strong colocalization with sox9a-expressing cartilages (not shown). Previously, we described the expression of hdac4 in the ventral region of the developing pharyngeal skeleton at 72 hpf (DeLaurier et al., 2012), and here we show how specific regions of expression are associated with sites of ossification of cartilage. By 72 hpf, expression is localized to regions of sox9a-expressing cartilage as well as in tissue surrounding cartilage and dermal bone elements. Co-expression of hdac4 and sox9a is detected in the hyosymplectic, ceratohyal, and palatoquadrate cartilages (Figs. 3A-H, indicated by arrows). In the case of the hyosymplectic and ceratohyal, co-expression of hdac4 and sox9a is in regions that will undergo ossification at later stages. hdac4 is strongly expressed in the posterior pharyngeal arches, overlapping in the mid-region of each arch with a domain of sox9a expression in the ceratobranchial cartilage within each arch (Figs. 3I-L).

Mutants have changes in expression of factors associated with onset of

ossification

MEF2C is known to activate transcription of *Runx2*, a transcription factor that activates chondrocyte maturation (Arnold et al., 2007). Runx2 in turn activates *Sp7*, a transcription factor associated with osteoblast differentiation (Nishio et al., 2006). We examined how loss of Hdac4, which would lead to over-activity of Mef2c, affects levels



296

297

298

299

300

301

302

303

304

305

306

307

308

309

310

311

of mRNA expression of these factors. Among teleost fish, a whole genome duplication event generated two copies of vertebrate runx2, runx2a and runx2b (van der Meulen et al., 2005). As in previous studies, we observed differential patterns of expression of both genes, indicating that these genes have unique functions in skeletal development in zebrafish (Fig. 4B and F). At 4 dpf, runx2a and runx2b are expressed in the mid-shaft region of the ceratohyal cartilage and branchiostegal ray (Fig. 4B and F), and also in the opercle (not shown). runx2b was also expressed in the hyosymplectic at this stage, but runx2a was not (not shown). In hdac4aik3/aik3 mutants, there is an increase in runx2a expression in the ceratohyal compared to wild type siblings (Fig. 4B-D, indicated by arrows, M, N). In mutants runx2a expression in the ceratohyal cartilage is broader, encompassing more length of the ceratohyal compared to wild type siblings, and expression is stronger (Fig. 4B-D, indicated by arrows, M, N). Expression of runx2b in hdac4aik3/aik3 mutants appears the same as in wild type siblings (Fig. 4E-H, indicated by arrows, M, N). At 4 dpf, in both wild types and mutants, sp7 expression is located as a small region of expression on the lateral aspect of the mid-shaft of the ceratohyal near the branchiostegal ray in both wild type and mutant larvae. Compared to wild types, expression of sp7 is increased in hdac4aik3/aik3 mutants (Fig. 4I-L, indicated by arrows, M, N).

313

314

315

316

317

312

Maternal-zygotic mutants have increased ossification of the pharyngeal skeleton

and defects in the anterior facial region

At 7 dpf, a subset of maternal zygotic mutants and heterozygotes showed a prominent

increase in cartilage ossification compared to wild types (non-sibling controls) (Fig. 5A-





318	G). In total, 40.0% (16/40) of maternal zygotic mutants and 40.0% (16/40)
319	heterozygotes had precocious ossification, including formation of an anguloarticular (aa)
320	bone associated with the Meckel's cartilage (Figs. 5B-D, G), an enlarged quadrate (see
321	Fig. 2A for reference, Fig. 5B), a dorsal hypohyal element (hhd) associated with the
322	ceratohyal (Figs. 5B and D), ossification of the symplectic of the hyosymplectic (Fig. 5B,
323	indicated by asterisk), and ossification of the mid-shaft of the first or first and second
324	ceratobranchial cartilages (Figs. 5C, D, F). Among maternal zygotic mutants, 25.9%
325	(15/58) had defects associated with loss of the first pharyngeal arch, including a
326	shortened face (Figs. 5G-J) and loss of one or both Meckel's cartilages and the anterior
327	portion of the palatoquadrate cartilage, along with retention of a small remnant of the
328	entopterygoid and quadrate (Fig. 5J, see Fig. 2A for reference). Among maternal
329	zygotic heterozygotes, 10.2% (6/59, Fig. 5G) also had loss of first arch structures. In the
330	case of larvae with a loss of first arch cartilages, posterior second arch and more
331	posterior arch structures including the ceratohyal, branchiostegal ray, and opercle were
332	present (Fig. 5J). Maternal zygotic mutants and heterozygotes also had defects in the
333	neurocranium cartilage (the primary palate in fish), including clefts, holes, and
334	shortening of the anterior portion of the element (Fig. 5K representative heterozygote
335	with normal neurocranium, L-M heterozygote and mutant with neurocranium defects). In
336	total, 30.8% (16/52) of maternal zygotic mutants, and 15.2% (7/46) of maternal zygotic
337	heterozygotes had neurocranium defects (Fig. 5G). Most neurocranium defects
338	occurred in fish which also had loss of first arch structures (11/16, 68.8% of maternal
339	zygotic mutants, and 5/7, 71.4% of maternal zygotic heterozygotes).
340	



342

343

344

345

346

347

348

349

350

351

352

353

354

355

356

357

358

359

360

361

362

363

Discussion

In this study, we generated two novel zebrafish lines with germ line mutations near the start of *hdac4*. Both lines have insertions that cause frameshifts and premature stop codons, which we predict causes truncated proteins with no functional Mef2c binding domain or HDAC domain. Although a CtBP domain may exist in a truncated form of the mutant protein, we do not think this is sufficient to preserve function of the Hdac4 protein as a repressor of ossification in the absence of the Mef2c and HDAC domains. RT-PCR and cDNA analysis does not reveal any alternative splice forms of the transcript, so we do not believe there is evidence for alternate versions of this protein caused by exon skipping or alternative splicing (Sharpe & Cooper, 2017). The presence of RT-PCR bands of the predicted size in mutants also indicates that transcripts are not subject to nonsense-mediated decay, and so it is unlikely that there is a trigger for a genetic compensatory response in mutants that could result in a less severe phenotype (El-Brolosy & Stainier, 2017). Analysis of zygotic mutants revealed a mild to moderate but statistically significant increase in ossification of the ceratohyal cartilage in both lines examined. One line showed a trend towards increased ossification of the hyosymplectic (hdac4aik2/aik2), although the increase in bone was not significant in mutants compared to wild type siblings. Normally, the hyosymplectic is the first element to commence ossification 4-5 dpf, followed by the ceratohyal by 6 dpf (Eames et al., 2013). In the case of the ceratohyal, ossification normally begins on the anterior margin of the midshaft of the element and extends posteriorly and along the length of the cartilage

element until around 12 dpf when the proximal end of the ceratohyal ossifies to form the



epihyal and the distal end of the ceratohyal ossifies to form the dorsal hypohyal (Cubbage & Mabee, 1996; Eames et al., 2013). Increased ossification of the ceratohyal in zygotic mutants resembles the pattern observed in 12-14 dpf wild type zebrafish (Eames et al., 2013), indicating that the ossification program in mutants is either precocious or is over-activated due to loss of Hdac4. Previous studies in the *Hdac4* mutant mouse show precocious ossification of the endochondral skeleton, with particular enhancement of ossification of chondral rib elements and limb cartilages in newborns (Vega et al., 2004). In both the mouse and the zebrafish, ossification of elements is not ectopic, but rather appears to reveal a premature onset of the ossification process.

In mouse Hdac4 mutants, Runx2 expression is increased in cartilage, and is associated with the increase of endochondral ossification of elements (Vega et al., 2004). In zebrafish, orthologs of *runx2*, *runx2a* and *runx2b* are both expressed in embryonic and larval cartilage and bone, consistent with a function in ossification (Flores et al., 2004; Li et al., 2009; van der Velden et al., 2013). At 48-96 hpf, *runx2a* is expressed in the maxilla, dentary, ceratohyal, opercle, and branchiostegal ray elements of the pharyngeal skeleton (Flores et al., 2004; Li et al., 2009; van der Velden et al., 2013). At 48-96 hpf, *runx2b* is expressed in the ceratohyal, hyosymplectic, parasphenoid, entopterygoid, opercle, branchiostegal ray, and ceratobranchial cartilages of the third to seventh pharyngeal arches (Flores et al., 2004; Li et al., 2009; van der Velden et al., 2013). These subtly different expression patterns indicate that following the teleost whole genome duplication approximately 300 million years ago (Amores et al., 1998; Hoegg et al., 2004), orthologs have similar but divergent functions



in zebrafish development. We observed increased expression of *runx2a* in *hdac4*-mutant zebrafish compared to wild types, which we hypothesize is due to a derepression of Mef2c function leading to increased transcription of *runx2a*. We did not observe any change in *runx2b* expression in mutants compared to wild types, potentially indicating that *runx2b* expression is not affected by loss of Hdac4 and increased function of Mef2c. Phylogenetic analysis indicates that *runx2a* and *runx2b* are divergent paralogs, and thus may be regulated by different factors in zebrafish (van der Meulen et al., 2005). The observation of a differential response in *runx2* paralog expression in *hdac4* mutants may reveal that *runx2a* and *runx2b* are regulated differently by Mef2c. We demonstrated an increase in *sp7* expression in the ceratohyal of *hdac4* mutants, which we hypothesize underlies the increased bone formation we observed in mutants, and may be up-regulated as a consequence of the increase in *runx2a* observed in mutants.

Maternal-zygotic mutants and heterozygotes showed an enhancement of the ossification phenotype observed in zygotic mutants. In addition to the increased ossification of the ceratohyal observed in zygotic mutants, 40% of maternal-zygotic mutants and heterozygotes had additional premature ossification of other pharyngeal skeletal elements. At 7 dpf, these larvae had evidence of a dorsal hypohyal at the distal portion of the ceratohyal, ossification of the symplectic cartilage of the hyosymplectic element, and ossification of the anterior ceratobranchial cartilages. Ossification of the dorsal hypohyal and symplectic normally occurs around 12 dpf, and ceratobranchial around 13 dpf (Cubbage & Mabee, 1996; Eames et al., 2013), indicating that the ossification program in maternal-zygotic mutants and heterozygotes is accelerated.



411

412

413

414

415

416

417

418

419

420

421

422

423

424

425

426

427

428

429

430

431

432

Among maternal-zygotic mutants and heterozygotes, the presence of an anguloarticular bone associated with the Meckel's cartilage was also observed. This element is normally first observed at around 12 dpf in wild type zebrafish. Unlike the other elements showing premature ossification, this element is a dermal bone that forms without a cartilaginous precursor (Cubbage & Mabee, 1996). Other dermal bones appear to be unaffected in zygotic or maternal-zygotic hdac4 mutants, and dermal bones are reported to be unaffected in Hdac4 mutant mice (Vega et al., 2004). We cannot explain why this particular dermal bone appears precociously in hdac4 mutants; however, as it forms on the surface of the Meckel's cartilage, anguloarticular precursor cells may be responding to signals from the underlying Meckel's cartilage to commence formation of bone. As an aside, it was noted that the cartilage of maternal-zygotic mutants and heterozygotes with excessive ossification generally had weaker Alcian Blue stain, and chondrocytes appeared rounder and less well organized compared to wild type controls (Figs. 5C and D). These differences in chondrocyte morphology and cartilage matrix indicate that loss of Hdac4 may also affect chondrocytes or chondrogenesis. The profound increase in ossification in a subset of maternal-zygotic mutants and heterozygotes compared to zygotic mutants suggests that there is a maternal influence on the chondral ossification program in zebrafish through Hdac4. In zebrafish, the

maternal-zygotic transition (MZT) commences around 2 hpf (128 cells) where maternal

transcripts are degraded and the first waves of zygotic transcripts are generated

(Tadros & Lipshitz, 2009). Using the RNA-seq expression atlas data for zebrafish

(https://www.ebi.ac.uk/gxa/home), we found that the highest level of hdac4 mRNA

PeerJ reviewing PDF | (2018:07:29625:0:0:REVIEW 14 Jul 2018)



expression in zebrafish is between cleavage (2 cell) and blastula dome (over 1K cell stage), followed by very low expression of transcripts up to 3 dpf (larval protruding mouth), after which transcript levels increase (Fig. 6). Since the high levels of *hdac4* mRNA in embryos prior to 128-cell stage can only be maternal transcripts, we believe this shows that there is a role for maternal Hdac4 in early development, and that only several days later does zygotic Hdac4 function in development. From our experiments, it is unclear how early maternal *hdac4* may be affecting ossification of cartilage several days post-fertilization. However, it is possible that maternal Hdac4 protein is still present in cells several days following the MZT and can influence ossification, or alternately, maternal Hdac4 may establish an epigenetic environment or signaling cascade in very early embryos which has consequences on downstream skeletogenesis. Future experiments will establish the levels of maternal Hdac4 in zebrafish embryos and we will examine the function of maternal transcripts or proteins on skeletal development in larvae.

Previously, we reported that morpholino knockdown of *hdac4* causes loss of neural crest and neurocranium defects in zebrafish (DeLaurier et al., 2012). Our zygotic mutants do not show any evidence of this phenotype. However, approximately one quarter of *hdac4* maternal-zygotic mutants show neurocranium defects and a loss of first arch cartilages consistent with a role for Hdac4 in neural crest development. Given the proportion of approximately one quarter of maternal-zygotic mutants showing this effect, we believe there may be a dihybrid effect of another unknown gene influencing the phenotypic outcome of loss or reductions of Hdac4 on neural crest. Future experiments will establish the levels of specifically maternal Hdac4 in zebrafish embryos

457

458

459

460

461

462

463

464

465

466

467

468

469

470

471

472

473

474

475

476

477

478

and we will examine the function of maternal transcripts or proteins on neural crest patterning and skeletal development in embryos and larvae.

In mouse, loss of MEF2C causes impaired chondrocyte hypertrophy and loss of endochondral ossification due to the failure to activate Runx2 and Ihh targets (Arnold et al., 2007). In zebrafish, the pharyngeal development of mef2ca and mef2cb mutants has been previously described (Miller et al., 2007; DeLaurier et al., 2014). Mef2ca mutants have a profound fusion defect of dorsal and ventral first and second arch cartilages and an expanded opercle bone. Mef2ca regulates expression of dlx genes, hand2, and nkx3.2 (bapx1) targets downstream of Edn1, and it is proposed that changes to expression of these factors through loss of *mef2ca* results in the joint fusions and dorsal-ventral patterning defects in mutants (Miller et al., 2007). Single mef2cb mutants have normal pharyngeal patterning, with no evidence of fusions or expansions of skeletal elements, indicating that Mef2cb does not function in the same capacity as Mef2ca in the Edn1 pathway during pharyngeal development (Miller et al., 2007) DeLaurier et al., 2014). If the function of zebrafish Mef2ca and Mef2cb is conserved with MEF2C function in the mouse, it is predicted that loss of either or both genes combined would result in a loss of perichondral ossification of cartilage. Previous studies do not report a perichondral ossification defect in single homozygous mutants or in mef2ca+/-;mef2cb-/- or mef2c-/-;mef2c+/- fish, although in all cases, larvae were studied at 6dpf, not 7dpf, and cartilage ossification was not quantitatively measured (Miller et al., 2007; DeLaurier et al., 2014). It is possible that the reported absence of a cartilage ossification defect in either single mutant is due to functional redundancy of the Mef2c paralogs to induce perichondral ossification, and that complete loss of both genes could result in



499

500

501

ossification defects in mutants. Unfortunately, the combined double homozygous mutant 480 has a heart malformation by 48 hpf (Hinits et al., 2012) resulting in severe 481 developmental defects by larval stages (DeLaurier et al., 2014). Future studies should reexamine the function of *mef2c* genes in cartilage ossification. For the *mef2ca* mutant, 482 it would be difficult to compare cartilage ossification patterns with that of wild type 483 484 larvae, due to the nature of joint fusions and patterning defects in cartilage. However, 485 future studies could quantitatively study ossification in *mef2cb* single mutants, or in 486 combined mutants where one *mef2ca* allele is heterozygous (i.e. *mef2ca*+/-;*mef2cb*-/-) 487 and fish develop without cardiac abnormalities, as previously reported (DeLaurier et al., 488 2014). 489 **Conclusions** 490 491 In conclusion, this study shows that mutation of hdac4 in zebrafish causes excessive 492 ossification of the pharyngeal skeleton, consistent with previous findings in the mouse 493 (Vega et al., 2004), indicating a conserved function for Hdac4 among vertebrates. 494 Mutants have increased expression of the transcription factors runx2a and sp7. 495 activators of the skeletal ossification program, which we hypothesize are upregulated in 496 response to increased activity of Mef2c through loss of Hdac4. Maternal-zygotic 497 crosses, along with RNA-seg analysis indicate that maternal Hdac4 is an important

contributor to embryonic and larval development. Zebrafish hdac4 mutant lines may be

useful resources for future study of the function of hdac4 in development of the skeleton

or other tissues, potentially along with other class IIa hdac mutants (i.e. hdac5, hdac7,

and hdac9) which may be compensating in part for loss of Hdac4. Maternal-zygotic





502	hdac4 mutants and heterozygotes further offer novel insights into the role of maternal
503	transcripts or proteins on late-stage larval tissue patterning.
504	
505	Acknowledgements
506	We would like to thank Jared Talbot, Nathan Hancock, and Alec Jones for providing
507	feedback on drafts of this manuscript, Derek Zelmer and Virginia Shervette for
508	assistance with the statistical analysis, and the Busch-Nentwich lab for providing RNA-
509	seq data.
510	



Figure legends

_	1	1
Э	1	Z

513

514

515

516

517

518

519

520

521

522

523

524

525

526

527

528

529

530

531

532

533

511

Figure 1: Overview of CRISPR strategy and generation of *hdac4* mutant lines. A: Genomic structure of *hdac4* showing gRNA target associated with the protospacer adjacent motif (5'-NGG, PAM) upstream of the Mef2c binding domain sequence. The histone deacetylase domain sequence is at the 3' end of the gene. Green arrows indicate forward (exon 3F) and reverse (exon 6R) primers for RT-PCR and sequencing of cDNA. Red arrows indicate intronic genotyping primers (hdac4 F6, hdac4 R6) flanking exon 5. Intron 2/3 and 3/4 not to scale, indicated by hash marks. B: Alignment of wild type (*hdac4*+/+) with mutant cDNA sequence showing nucleotide insertions (blue) in hdac4aik2/aik2 and hdac4aik3/aik3 mutants in exon 5. C and D: Insertion of nucleotides results in reading frame shifts causing aberrant protein sequences (magenta in C, grey boxes in D), loss of the Mef2c binding domain (indicated in yellow in C), and premature termination of the protein sequence (asterisk in C indicates stop codon). E and F: RT-PCR showing *hdac4* cDNA is spliced correctly in mutants and there is no evidence of splice variants. The wild type cDNA product is expected to be 535 bp and mutant bands are 554 bp (hdac4aik2/aik2 in E) and 571 bp (hdac4aik3/aik3 in F). The larger band in hdac4aik3 mutants (indicated by white asterisk in F) was sequenced and determined to be identical to the lower band. G and H: Genomic DNA samples were genotyped by PCR and show differences in band sizes indicating mutant (841 bp hdac4aik2/aik2, 858 bp hdac4aik3/aik3), wild type (822bp), and heterozygous fish (mutant and wild type bands). I and J: At 7dpf, mutant hdac4aik3/aik3 fish (J) appear normal compared to wild type siblings (I). H_2O = negative control. 100 bp ladder.

5	2	1

Figure 2: Analysis of ossification of the pharyngeal skeleton of *hdac4* zygotic mutants. 535 536 A: Schematic showing elements of the 7 dpf larvae pharyngeal skeleton. Cartilage is indicated in blue, bone is indicated in red. B and C: Total scores assigned to 7 dpf 537 538 larvae scored for aik2 and aik3 lines, respectively. D and D': wild type larval pharyngeal 539 skeleton and enlarged view of ceratohyal. E and E': hdac4aik2 mutant larvae showing 540 "mild" increase of ossification of ceratohyal. Arrow indicates irregular border of 541 ossification and asterisk indicates bone collar on dorsal surface of ceratohyal. Lower 542 arrow indicates spread of ossification to ventral aspect of ceratohyal. F and F': hdac4aik2/aik2 mutant showing "moderate" increase of ossification of ceratohyal. Asterisks 543 544 indicate bone collar on dorsal and ventral surfaces of the ceratohyal. G and H: Bar graphs comparing ratios of bone to total area of the ceratohyal for aik2 and aik3. I and 545 546 J: Bar graphs comparing ratios of bone to total area of the hyosymplectic for aik2 and 547 aik3. For G-J, aik2 total fish = 93, including WT = 38, heterozygote = 23, and mutant = 32; aik3 total fish = 61, including WT = 17, heterozygote = 28, and mutant = 16. 548 549 Abbreviations: ch = ceratohyal, bsr = branchiostegal ray, de = dentary, en = 550 entopterygoid, hs = hyosymplectic, ih = interhyal, m = Meckel's cartilage, op = opercle, pq = palatoquadrate, q = quadrate. * p \leq 0.05, ** p \leq 0.01, *** p \leq 0.001. Scale bar = 100 551 552 microns. Cartilage is stained blue (Alcian Blue), bone is stained red (Alizarin Red). 553 554 Figure 3: Expression of *hdac4* and *sox9a* mRNA in the pharyngeal skeleton of wild type 555 embryos at 72 hpf. A: Schematic of skeletal elements, lateral view for B-D, blue 556 indicates cartilage, red indicates bone. B-D: expression of hdac4 and sox9a, arrows





557 indicate expression in hyosymplectic, ceratohyal, and palatoquadrate cartilages. E: 558 Schematic of skeletal elements, lateral view for F-H. F-H: expression of hdac4 and 559 sox9a, arrows indicate expression in ceratohyal and hyosymplectic cartilages. I: Schematic of skeletal elements, ventral view for J-L. J-L: expression of hdac4 and 560 561 sox9a, arrows indicate expression in the posterior pharyngeal arches. Abbreviations: bb 562 = basibranchial, ch = ceratohyal, hs = hyosymplectic, ih = interhyal, m = Meckel's cartilage, op = opercle, pa3-7 = posterior pharyngeal arches, pg = palatoguadrate. 563 564 Scale bar = 50 microns. 565 Figure 4: Expression of runx2a, runx2b, and sp7 mRNA in the pharyngeal skeleton of 566 wild-type and hdac4aik3/aik3 mutant larvae at 4 dpf. A, C, E, G, I, K: Schematic view of 567 skeletal elements, ventral view, blue indicates cartilage, red indicates bone. B and D: 568 569 expression of runx2a in wild type (B) and mutant (D), arrows indicate expression in the 570 ceratohyal. F and H: expression of runx2b in wild type (F) and mutant (H), arrows 571 indicate expression in the ceratohyal. J and L: expression of sp7 in wild type (J) and 572 mutant (L), arrows indicate expression in the ceratohyal. M: schematic showing 573 overlapping domains of expression of runx2a, runx2b, and sp7 in wild type larvae. N: 574 schematic showing expanded runx2a and sp7 domains in mutant larvae. Abbreviations: 575 ch = ceratohyal, bsr = branchiostegal ray, pa3 = pharyngeal arch 3, pq = 576 palatoquadrate. Scale bar = 50 microns. 577 578 Figure 5: Analysis of maternal-zygote mutant and heterozygote skeletal patterning. A: 579 Wild type (non-sibling) larval pharyngeal skeleton at 7 dpf. B-D: maternal-zygotic mutant





580	(B and C) and heterozygote (D) pharyngeal skeletons at 7 dpf showing precocious
581	angular articular bone (aa, indicated in B and C), dorsal hypohyal (hhd, indicated in B
582	and D), ossification of the symplectic of the hyosymplectic (indicated by asterisk in B).
583	E: Wild type posterior pharyngeal arches 3 and 4 showing first and second
584	ceratobranchial cartilages (cb1, cb2), ventral view, 7 dpf. F: maternal-zygotic mutant
585	showing ossification of the ceratobranchial cartilages, indicated by arrows (also in C). G
586	Total scores of maternal zygotic mutants and heterozygotes for first arch (M, Pq defect)
587	neurocranium, and early ossification defects. H: Maternal-zygotic heterozygote at 72
588	hpf, lateral view. I: Maternal-zygotic mutant at 72 hpf, lateral view. J: Maternal-zygotic
589	mutant showing loss of first arch cartilage, a small remnant entopterygoid bone (en) and
590	quadrate (q) associated with the palatoquadrate are present (see Fig. 2A for reference).
591	K and L: Maternal-zygotic heterozygote neurocrania, ventral view, 7 dpf. L: Maternal-
592	zygotic mutant neurocranium, ventral view, 7 dpf. A-D, H-M: Scale bar = 200 microns, E
593	and F: Scale bar = 50 microns. Cartilage is stained blue (Alcian Blue), bone is stained
594	red (Alizarin Red).
595	
596	Figure 6: RNA-seq mRNA levels of <i>hdac4</i> transcripts from zygotic to larval day 5 stage.
597	Bars indicate numbers of <i>hdac4</i> transcripts per million transcripts read at each stage.
598	Between the 128 and 256-cell stage, maternal transcripts degrade and zygotic
599	transcripts become predominant. See http://www.ebi.ac.uk/gxa/experiments/E-ERAD-
600	475 for Expression Atlas data.
601	
602	







References

605

606	
607	Amores A., Force A., Yan YL., Joly L., Amemiya C., Fritz A., Ho RK., Langeland J.,
608	Prince V., Wang YL., Westerfield M., Ekker M., Postlethwait JH. 1998. Zebrafish
609	hox clusters and vertebrate genome evolution. Science (New York, N.Y.)
610	282:1711–1714.
611	Arnold MA., Kim Y., Czubryt MP., Phan D., McAnally J., Qi X., Shelton JM., Richardson
612	JA., Bassel-Duby R., Olson EN. 2007. MEF2C transcription factor controls
613	chondrocyte hypertrophy and bone development. Developmental Cell 12:377-
614	389. DOI: 10.1016/j.devcel.2007.02.004.
615	Avaron F., Hoffman L., Guay D., Akimenko MA. 2006. Characterization of two new
616	zebrafish members of the hedgehog family: Atypical expression of a zebrafish
617	indian hedgehog gene in skeletal elements of both endochondral and dermal
618	origins. Developmental Dynamics 235:478–489. DOI: 10.1002/dvdy.20619.
619	Bassett AR., Tibbit C., Ponting CP., Liu J-L. 2013. Highly Efficient Targeted
620	Mutagenesis of Drosophila with the CRISPR/Cas9 System. Cell Reports 4:220-
621	228. DOI: 10.1016/j.celrep.2013.06.020.
622	Cubbage CC., Mabee PM. 1996. Development of the cranium and paired fins in the
623	zebrafish Danio rerio (Ostariophysi, Cyprinidae). Journal of Morphology 229:121-
624	160. DOI: 10.1002/(SICI)1097-4687(199608)229:2<121::AID-JMOR1>3.0.CO;2-
625	4.
626	DeLaurier A., Eames BF., Blanco-Sánchez B., Peng G., He X., Swartz ME., Ullmann B.
627	Westerfield M., Kimmel CB. 2010. Zebrafish sp7:EGFP: a transgenic for studying



628	otic vesicle formation, skeletogenesis, and bone regeneration. Genesis (New
629	York, N.Y.: 2000) 48:505-511. DOI: 10.1002/dvg.20639.
630	DeLaurier A., Huycke TR., Nichols JT., Swartz ME., Larsen A., Walker C., Dowd J., Pan
631	L., Moens CB., Kimmel CB. 2014. Role of mef2ca in developmental buffering of
632	the zebrafish larval hyoid dermal skeleton. Developmental Biology 385:189–199.
633	DOI: 10.1016/j.ydbio.2013.11.016.
634	DeLaurier A., Nakamura Y., Braasch I., Khanna V., Kato H., Wakitani S., Postlethwait
635	JH., Kimmel CB. 2012. Histone deacetylase-4 is required during early cranial
636	neural crest development for generation of the zebrafish palatal skeleton. BMC
637	developmental biology 12:16. DOI: 10.1186/1471-213X-12-16.
638	Eames BF., DeLaurier A., Ullmann B., Huycke TR., Nichols JT., Dowd J., McFadden M.,
639	Sasaki MM., Kimmel CB. 2013. FishFace: interactive atlas of zebrafish
640	craniofacial development at cellular resolution. BMC developmental biology
641	13:23. DOI: 10.1186/1471-213X-13-23.
642	El-Brolosy MA., Stainier DYR. 2017. Genetic compensation: A phenomenon in search
643	of mechanisms. PLoS genetics 13:e1006780. DOI:
644	10.1371/journal.pgen.1006780.
645	Flores MV., Tsang VWK., Hu W., Kalev-Zylinska M., Postlethwait J., Crosier P., Crosier
646	K., Fisher S. 2004. Duplicate zebrafish runx2 orthologues are expressed in
647	developing skeletal elements. Gene Expression Patterns 4:573–581. DOI:
648	10.1016/j.modgep.2004.01.016.



649	Gao B., Guo J., She C., Shu A., Yang M., Tan Z., Yang X., Guo S., Feng G., He L.
650	2001. Mutations in IHH, encoding Indian hedgehog, cause brachydactyly type A-
651	1. Nature Genetics 28:386–388. DOI: 10.1038/ng577.
652	Haberland M., Montgomery RL., Olson EN. 2009. The many roles of histone
653	deacetylases in development and physiology: implications for disease and
654	therapy. Nature Reviews. Genetics 10:32–42. DOI: 10.1038/nrg2485.
655	Hall BK. 2014. Bones and Cartilage: Developmental and Evolutionary Skeletal Biology.
656	Academic Press.
657	Hinits Y., Pan L., Walker C., Dowd J., Moens CB., Hughes SM. 2012. Zebrafish Mef2ca
658	and Mef2cb are essential for both first and second heart field cardiomyocyte
659	differentiation. Developmental biology 369:199–210. DOI:
660	10.1016/j.ydbio.2012.06.019.
661	Hoegg S., Brinkmann H., Taylor JS., Meyer A. 2004. Phylogenetic timing of the fish-
662	specific genome duplication correlates with the diversification of teleost fish.
663	Journal of Molecular Evolution 59:190–203. DOI: 10.1007/s00239-004-2613-z.
664	Huycke TR., Eames BF., Kimmel CB. 2012. Hedgehog-dependent proliferation drives
665	modular growth during morphogenesis of a dermal bone. Development
666	(Cambridge, England) 139:2371–2380. DOI: 10.1242/dev.079806.
667	Hwang WY., Fu Y., Reyon D., Maeder ML., Tsai SQ., Sander JD., Peterson RT., Yeh J-
668	RJ., Joung JK. 2013. Efficient genome editing in zebrafish using a CRISPR-Cas
669	system. Nature Biotechnology 31:227–229. DOI: 10.1038/nbt.2501.
670	Karsenty G., Wagner EF. 2002. Reaching a genetic and molecular understanding of
671	skeletal development. Developmental Cell 2:389–406.



Kearse M., Moir R., Wilson A., Stones-Havas S., Cheung M., Sturrock S., Buxton S.,
Cooper A., Markowitz S., Duran C., Thierer T., Ashton B., Meintjes P.,
Drummond A. 2012. Geneious Basic: an integrated and extendable desktop
software platform for the organization and analysis of sequence data.
Bioinformatics (Oxford, England) 28:1647–1649. DOI:
10.1093/bioinformatics/bts199.
Komori T., Yagi H., Nomura S., Yamaguchi A., Sasaki K., Deguchi K., Shimizu Y.,
Bronson RT., Gao YH., Inada M., Sato M., Okamoto R., Kitamura Y., Yoshiki S.,
Kishimoto T. 1997. Targeted disruption of Cbfa1 results in a complete lack of
bone formation owing to maturational arrest of osteoblasts. Cell 89:755–764.
Labun K., Montague TG., Gagnon JA., Thyme SB., Valen E. 2016. CHOPCHOP v2: a
web tool for the next generation of CRISPR genome engineering. Nucleic Acids
Research 44:W272-W276. DOI: 10.1093/nar/gkw398.
Li N., Felber K., Elks P., Croucher P., Roehl HH. 2009. Tracking gene expression during
zebrafish osteoblast differentiation. Developmental Dynamics: An Official
Publication of the American Association of Anatomists 238:459–466. DOI:
10.1002/dvdy.21838.
Lu J., McKinsey TA., Nicol RL., Olson EN. 2000. Signal-dependent activation of the
MEF2 transcription factor by dissociation from histone deacetylases.
Proceedings of the National Academy of Sciences of the United States of
America 97:4070–4075. DOI: 10.1073/pnas.080064097.
Maeda Y., Nakamura E., Nguyen M-T., Suva LJ., Swain FL., Razzaque MS., Mackem
S., Lanske B. 2007. Indian Hedgehog produced by postnatal chondrocytes is



195	essential for maintaining a growth plate and trabecular bone. Proceedings of the
96	National Academy of Sciences of the United States of America 104:6382–6387.
97	DOI: 10.1073/pnas.0608449104.
98	McKinsey TA., Zhang CL., Lu J., Olson EN. 2000. Signal-dependent nuclear export of a
99	histone deacetylase regulates muscle differentiation. Nature 408:106–111. DOI:
00	10.1038/35040593.
01	van der Meulen T., Kranenbarg S., Schipper H., Samallo J., van Leeuwen JL., Franssen
02	H. 2005. Identification and characterisation of two runx2 homologues in zebrafish
03	with different expression patterns. Biochimica Et Biophysica Acta 1729:105–117.
'04	DOI: 10.1016/j.bbaexp.2005.03.008.
05	Miller CT., Swartz ME., Khuu PA., Walker MB., Eberhart JK., Kimmel CB. 2007. mef2ca
'06	is required in cranial neural crest to effect Endothelin1 signaling in zebrafish.
07	Developmental Biology 308:144–157. DOI: 10.1016/j.ydbio.2007.05.018.
08	Montague TG., Cruz JM., Gagnon JA., Church GM., Valen E. 2014. CHOPCHOP: a
'09	CRISPR/Cas9 and TALEN web tool for genome editing. Nucleic Acids Research
10	42:W401–W407. DOI: 10.1093/nar/gku410.
11	Nakashima K., Zhou X., Kunkel G., Zhang Z., Deng JM., Behringer RR., de
12	Crombrugghe B. 2002. The novel zinc finger-containing transcription factor
13	osterix is required for osteoblast differentiation and bone formation. Cell 108:17–
14	29.
15	Nishio Y., Dong Y., Paris M., O'Keefe RJ., Schwarz EM., Drissi H. 2006. Runx2-
16	mediated regulation of the zinc finger Osterix/Sp7 gene. Gene 372:62–70. DOI:
17	10.1016/j.gene.2005.12.022.



718	Passier R., Zeng H., Frey N., Naya FJ., Nicol RL., McKinsey TA., Overbeek P.,
719	Richardson JA., Grant SR., Olson EN. 2000. CaM kinase signaling induces
720	cardiac hypertrophy and activates the MEF2 transcription factor in vivo. The
721	Journal of Clinical Investigation 105:1395–1406. DOI: 10.1172/JCI8551.
722	Quack I., Vonderstrass B., Stock M., Aylsworth AS., Becker A., Brueton L., Lee PJ.,
723	Majewski F., Mulliken JB., Suri M., Zenker M., Mundlos S., Otto F. 1999.
724	Mutation analysis of core binding factor A1 in patients with cleidocranial
725	dysplasia. American Journal of Human Genetics 65:1268–1278.
726	Sharpe JJ., Cooper TA. 2017. Unexpected consequences: exon skipping caused by
727	CRISPR-generated mutations. Genome Biology 18:109. DOI: 10.1186/s13059-
728	017-1240-0.
729	Tadros W., Lipshitz HD. 2009. The maternal-to-zygotic transition: a play in two acts.
730	Development 136:3033–3042. DOI: 10.1242/dev.033183.
731	Talbot JC., Johnson SL., Kimmel CB. 2010. hand2 and Dlx genes specify dorsal,
732	intermediate and ventral domains within zebrafish pharyngeal arches.
733	Development (Cambridge, England) 137:2507–2517. DOI: 10.1242/dev.049700.
734	Truett GE., Heeger P., Mynatt RL., Truett AA., Walker JA., Warman ML. 2000.
735	Preparation of PCR-quality mouse genomic DNA with hot sodium hydroxide and
736	tris (HotSHOT). BioTechniques 29:52, 54.
737	Valadares ER., Carneiro TB., Santos PM., Oliveira AC., Zabel B. 2014. What is new in
738	genetics and osteogenesis imperfecta classification? Jornal De Pediatria 90:536-
739	541. DOI: 10.1016/j.jped.2014.05.003.

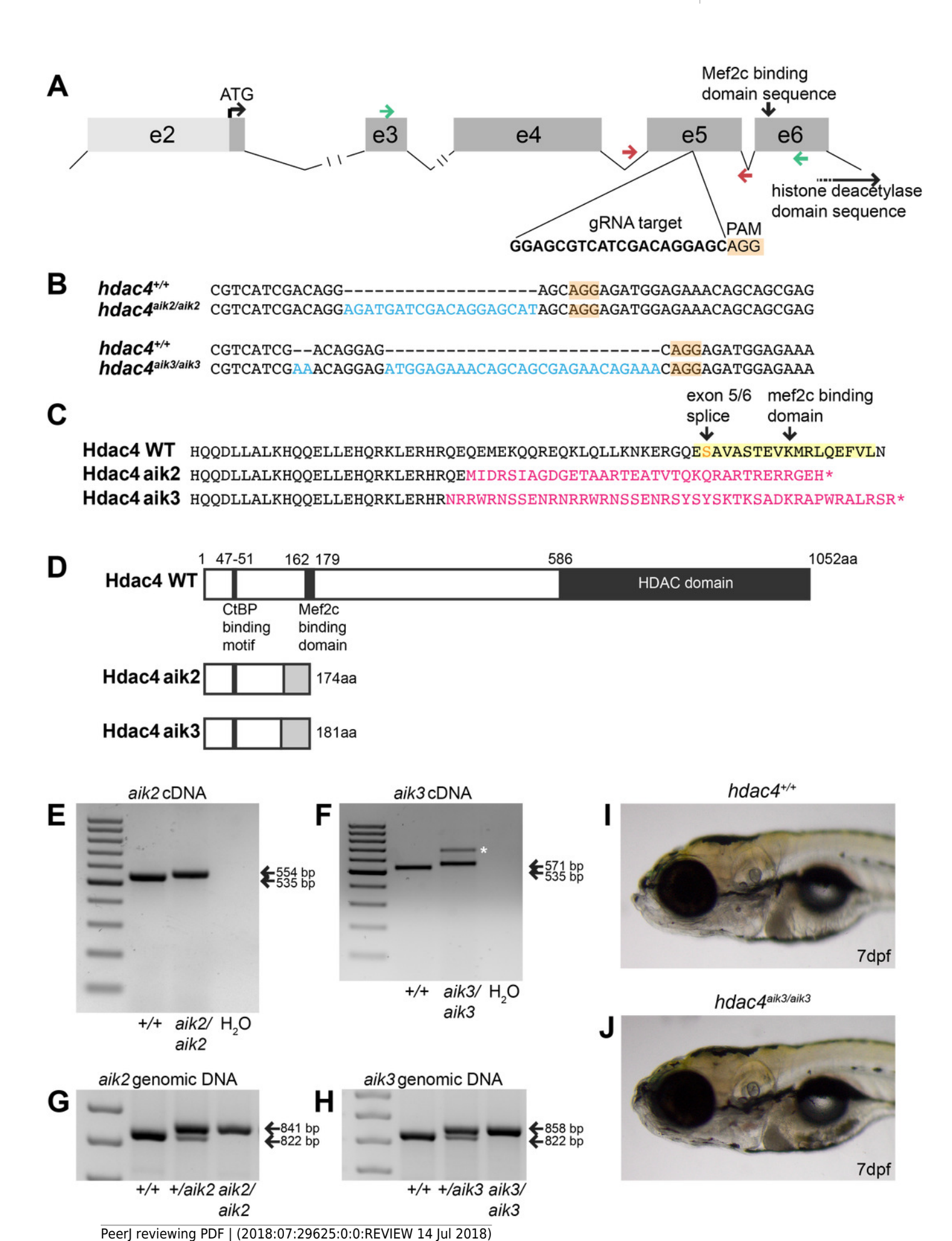


740	Vega RB., Matsuda K., Oh J., Barbosa AC., Yang X., Meadows E., McAnally J.,
741	Pomajzl C., Shelton JM., Richardson JA., Karsenty G., Olson EN. 2004. Histone
742	deacetylase 4 controls chondrocyte hypertrophy during skeletogenesis. Cell
743	119:555–566. DOI: 10.1016/j.cell.2004.10.024.
744	van der Velden YU., Wang L., Querol Cano L., Haramis A-PG. 2013. The polycomb
745	group protein ring1b/rnf2 is specifically required for craniofacial development.
746	PloS One 8:e73997. DOI: 10.1371/journal.pone.0073997.
747	Vortkamp A., Lee K., Lanske B., Segre GV., Kronenberg HM., Tabin CJ. 1996.
748	Regulation of rate of cartilage differentiation by Indian hedgehog and PTH-
749	related protein. Science (New York, N.Y.) 273:613-622.
750	Walker MB., Kimmel CB. 2007. A two-color acid-free cartilage and bone stain for
751	zebrafish larvae. Biotechnic & Histochemistry: Official Publication of the
752	Biological Stain Commission 82:23–28. DOI: 10.1080/10520290701333558.
753	Wasden MB., Roberts RL., DeLaurier A. 2017. Optimizing Sperm Collection Procedures
754	in Zebrafish. Journal of the South Carolina Academy of Science 15.
755	Wysolmerski JJ., Cormier S., Philbrick WM., Dann P., Zhang JP., Roume J., Delezoide
756	AL., Silve C. 2001. Absence of functional type 1 parathyroid hormone
757	(PTH)/PTH-related protein receptors in humans is associated with abnormal
758	breast development and tooth impaction. The Journal of Clinical Endocrinology
759	and Metabolism 86:1788–1794. DOI: 10.1210/jcem.86.4.7404.
760	



Overview of CRISPR strategy and generation of hdac4 mutant lines.

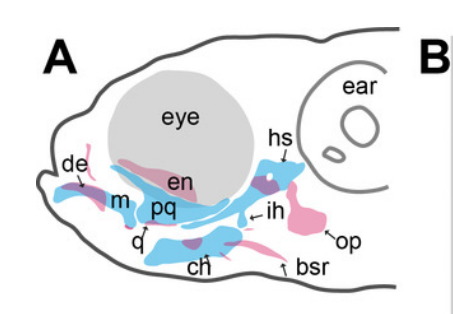
A: Genomic structure of hdac4 showing gRNA target associated with the protospacer adjacent motif (5'-NGG, PAM) upstream of the Mef2c binding domain sequence. The histone deacetylase domain sequence is at the 3' end of the gene. Green arrows indicate forward (exon 3F) and reverse (exon 6R) primers for RT-PCR and sequencing of cDNA. Red arrows indicate intronic genotyping primers (hdac4 F6, hdac4 R6) flanking exon 5. Intron 2/3 and 3/4 not to scale, indicated by hash marks. B: Alignment of wild type (hdac4+/+) with mutant cDNA sequence showing nucleotide insertions (blue) in hdac4aik2/aik2 and hdac4aik3/aik3 mutants in exon 5. C and D: Insertion of nucleotides results in reading frame shifts causing aberrant protein sequences (magenta in C, grey boxes in D), loss of the Mef2c binding domain (indicated in yellow in C), and premature termination of the protein sequence (asterisk in C indicates stop codon). E and F: RT-PCR showing *hdac4* cDNA is spliced correctly in mutants and there is no evidence of splice variants. The wild type cDNA product is expected to be 535 bp and mutant bands are 554 bp (hdac4aik2/aik2 in E) and 571 bp (hdac4aik3/aik3 in F). The larger band in hdac4aik3/aik3 mutants (indicated by white asterisk in F) was sequenced and determined to be identical to the lower band. G and H: Genomic DNA samples were genotyped by PCR and show differences in band sizes indicating mutant (841 bp hdac4aik2/aik2, 858 bp hdac4aik3/aik3), wild type (822bp), and heterozygous fish (mutant and wild type bands). I and J: At 7dpf, mutant $hdac4^{aik3/aik3}$ fish (I) appear normal compared to wild type siblings (I). H_2O = negative control. 100 bp ladder.





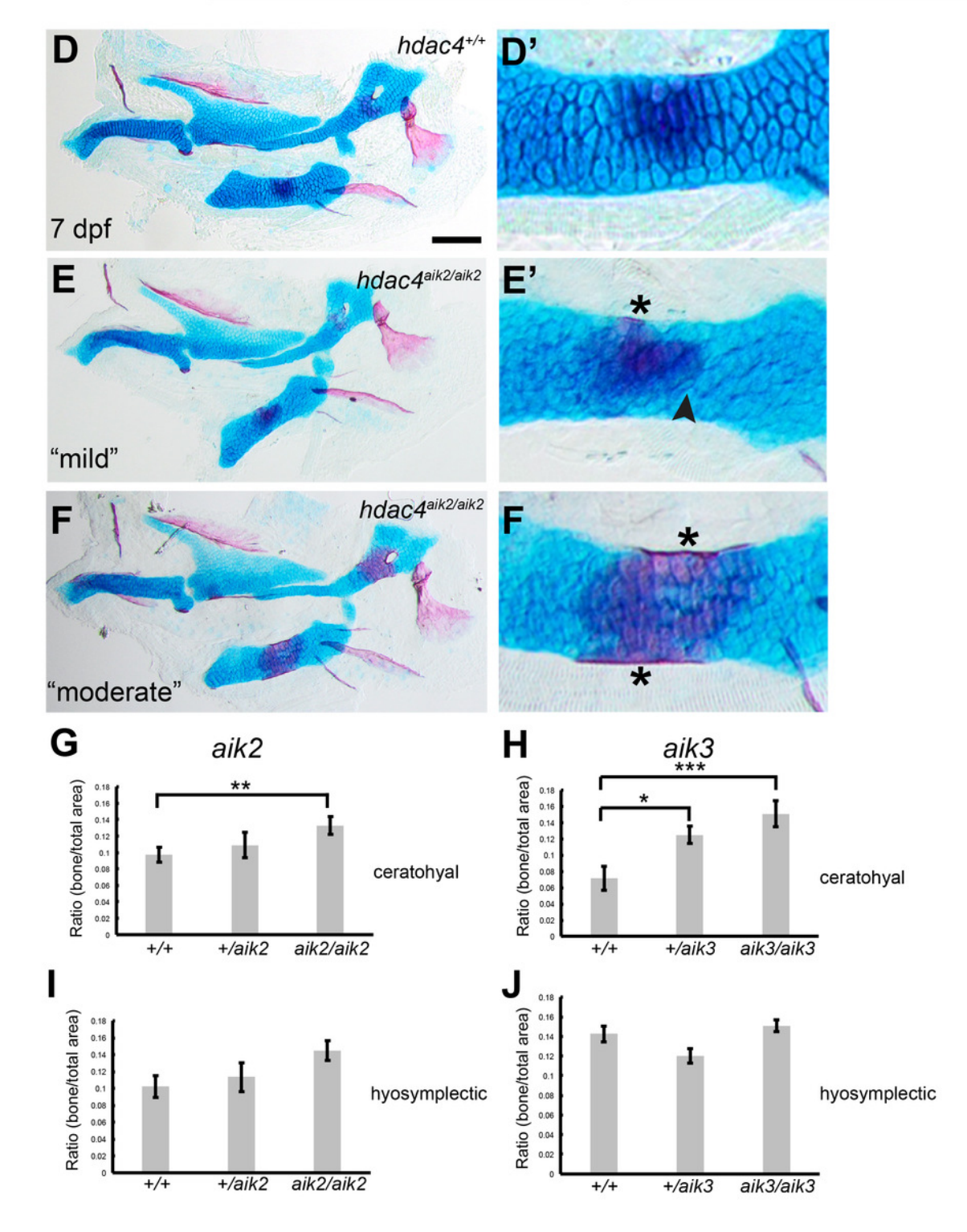
Analysis of ossification of the pharyngeal skeleton of hdac4 zygotic mutants.

A: Schematic showing elements of the 7 dpf larvae pharyngeal skeleton. Cartilage is indicated in blue, bone is indicated in red. B and C: Total scores assigned to 7 dpf larvae scored for aik2 and aik3 lines, respectively. D and D': wild type larval pharyngeal skeleton and enlarged view of ceratohyal. E and E': $hdac4^{aik2/aik2}$ mutant larvae showing "mild" increase of ossification of ceratohyal. Arrow indicates irregular border of ossification and asterisk indicates bone collar on dorsal surface of ceratohyal. Lower arrow indicates spread of ossification to ventral aspect of ceratohyal. F and F': $hdac4^{aik2/aik2}$ mutant showing "moderate" increase of ossification of ceratohyal. Asterisks indicate bone collar on dorsal and ventral surfaces of the ceratohyal. G and H: Bar graphs comparing ratios of bone to total area of the ceratohyal for aik2 and aik3. I and J: Bar graphs comparing ratios of bone to total area of the hyosymplectic for aik2 and aik3. Abbreviations: ch = ceratohyal, ch =



	normal	mild	moderate
hdac4*/+	26/38 (68.4%)	12/38 (31.6%)	0/38 (0%)
hdac4 ^{+/aik2}	12/23	6/23	5/23
	(52.2%)	(26.1%)	(21.7%)
hdac4 ^{aik2/aik2}	9/32	11/32	12/32
	(28.1%)	(34.4%)	(37.5%)

,	normal	mild	moderate
hdac4*/*	23/26	3/26	0/26
	(88.5%)	(11.5%)	(0%)
hdac4+/aik3	36/52	12/52	4/52
	(69.2%)	(23.1%)	(7.7%)
hdac4aik3/aik3	9/33	21/33	3/33
	(27.3%)	(63.6%)	(9.1%)



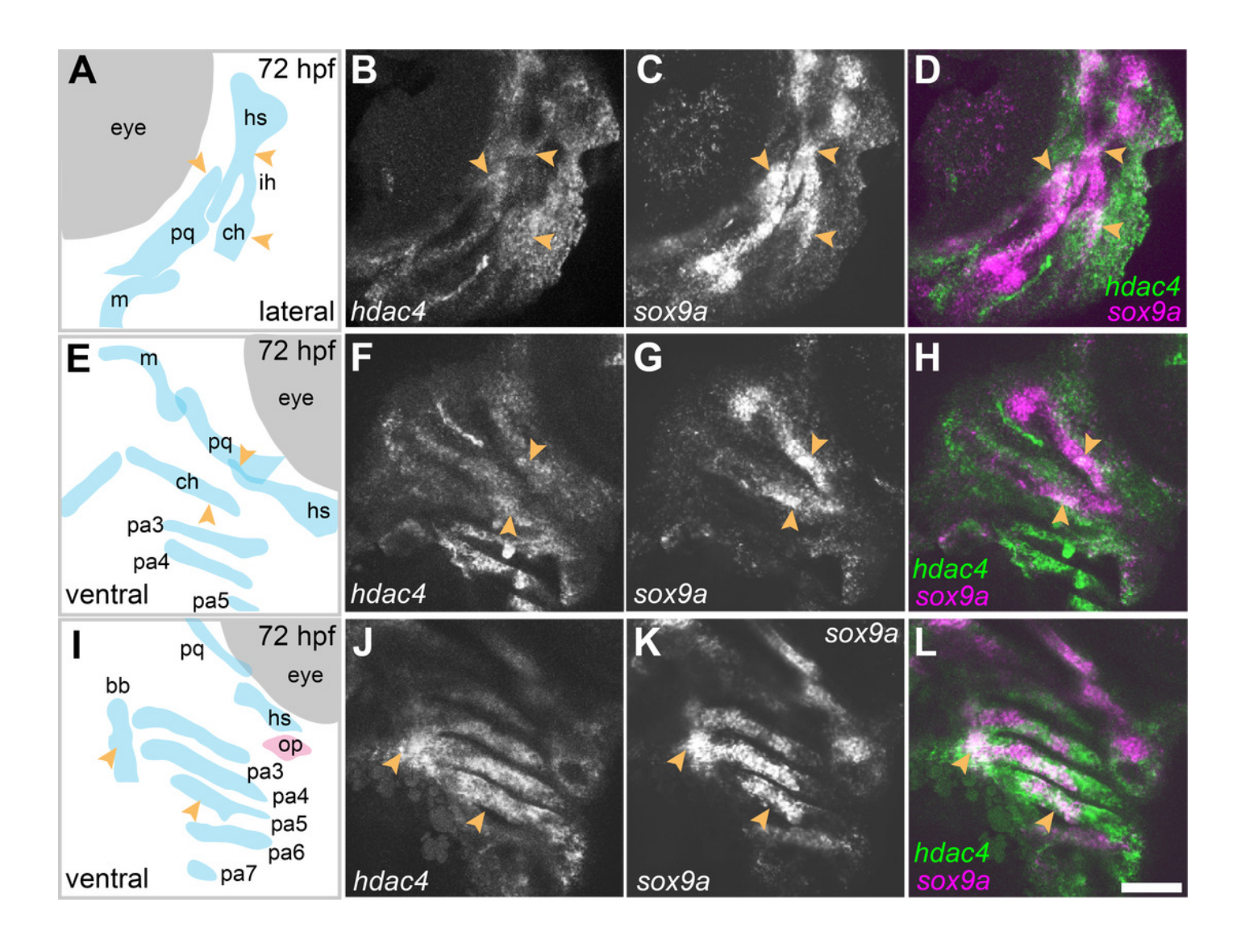


Expression of *hdac4* and *sox9a* mRNA in the pharyngeal skeleton of wild type embryos at 72 hpf.

A: Schematic of skeletal elements, lateral view for B-D, blue indicates cartilage, red indicates bone. B-D: expression of *hdac4* and *sox9a*, arrows indicate expression in hyosymplectic, ceratohyal, and palatoquadrate cartilages. E: Schematic of skeletal elements, lateral view for F-H. F-H: expression of *hdac4* and *sox9a*, arrows indicate expression in ceratohyal and hyosymplectic cartilages. I: Schematic of skeletal elements, ventral view for J-L. J-L: expression of *hdac4* and *sox9a*, arrows indicate expression in the posterior pharyngeal arches. Abbreviations: bb = basibranchial, ch = ceratohyal, hs = hyosymplectic, ih = interhyal, m = Meckel's cartilage, op = opercle, pa3-7 = posterior pharyngeal arches, pq = palatoquadrate. Scale bar = 50 microns.

*Note: Auto Gamma Correction was used for the image. This only affects the reviewing manuscript. See original source image if needed for review.



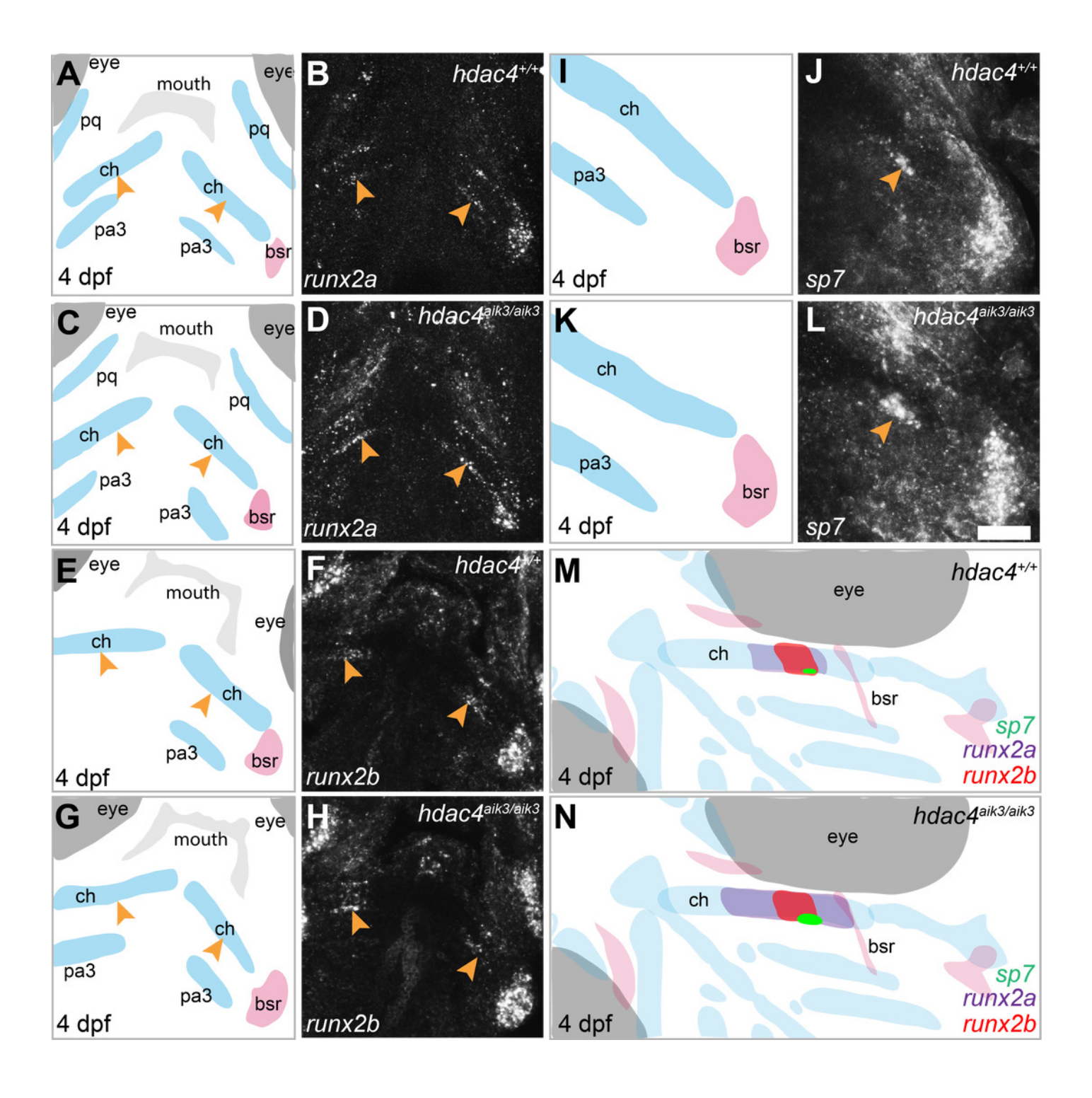




Expression of *runx2a*, *runx2b*, and *sp7* mRNA in the pharyngeal skeleton of wild-type and *hdac4*^{aik3/aik3} mutant larvae at 4 dpf.

A, C, E, G, I, K: Schematic view of skeletal elements, ventral view, blue indicates cartilage, red indicates bone. B and D: expression of runx2a in wild type (B) and mutant (D), arrows indicate expression in the ceratohyal. F and H: expression of runx2b in wild type (F) and mutant (H), arrows indicate expression in the ceratohyal. J and L: expression of sp7 in wild type (J) and mutant (L), arrows indicate expression in the ceratohyal. M: schematic showing overlapping domains of expression of runx2a, runx2b, and sp7 in wild type larvae. N: schematic showing expanded runx2a and sp7 domains in mutant larvae. Abbreviations: ch = ceratohyal, bsr = branchiostegal ray, pa3 = pharyngeal arch 3, pq = palatoquadrate. Scale bar = 50 microns.

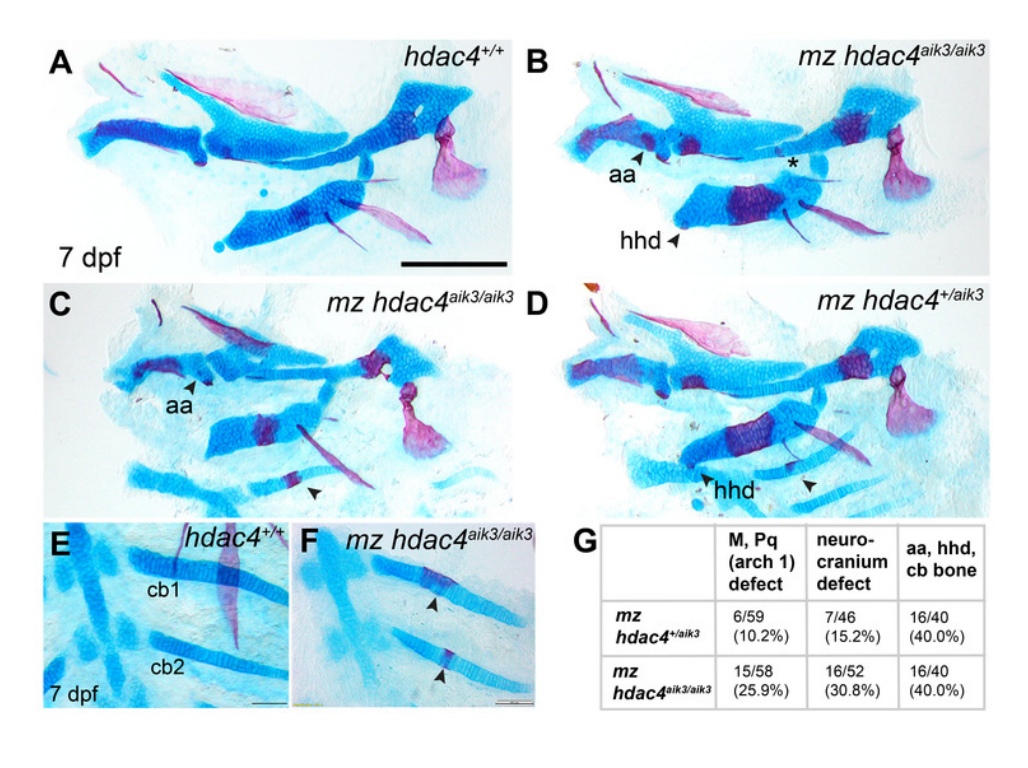


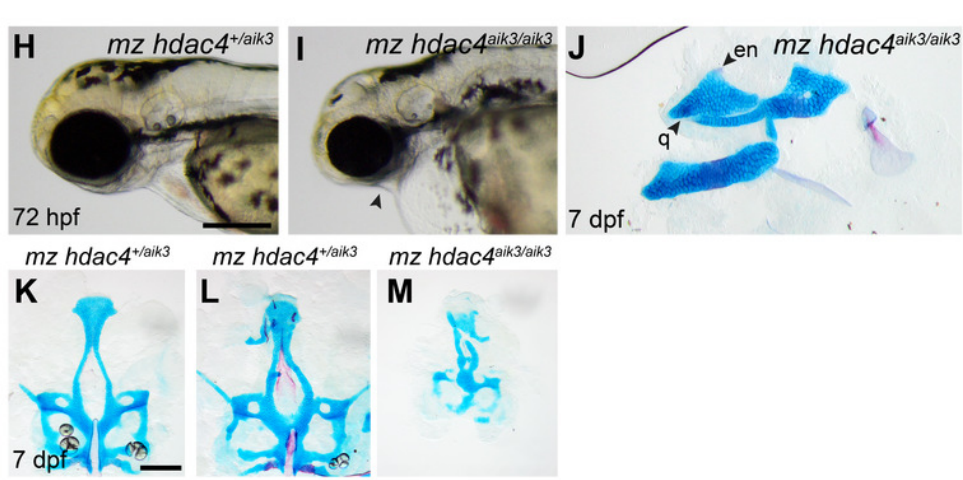


Analysis of maternal-zygote mutant and heterozygote skeletal patterning

A: Wild type (non-sibling) larval pharyngeal skeleton at 7 dpf. B-D: maternal-zygotic mutant (B and C) and heterozygote (D) pharyngeal skeletons at 7 dpf showing precocious angular articular bone (aa, indicated in B and C), dorsal hypohyal (hhd, indicated in B and D), ossification of the symplectic of the hyosymplectic (indicated by asterisk in B). E: Wild type posterior pharyngeal arches 3 and 4 showing first and second ceratobranchial cartilages (cb1, cb2), ventral view, 7 dpf. F: maternal-zygotic mutant showing ossification of the ceratobranchial cartilages, indicated by arrows (also in C). G: Total scores of maternal zygotic mutants and heterozygotes for first arch (M, Pq defect), neurocranium, and early ossification defects. H: Maternal-zygotic heterozygote at 72 hpf, lateral view. I: Maternal-zygotic mutant at 72 hpf, lateral view. J: Maternal-zygotic mutant showing loss of first arch cartilage, a small remnant entopterygoid bone (en) and quadrate (q) associated with the palatoquadrate are present (see Fig. 2A for reference). K and L: Maternal-zygotic heterozygote neurocrania, ventral view, 7 dpf. L: Maternal-zygotic mutant neurocranium, ventral view, 7 dpf. A-D, H-M: Scale bar = 200 microns, E and F: Scale bar = 50 microns. Cartilage is stained blue (Alcian Blue), bone is stained red (Alizarin Red).









RNA-seg mRNA levels of hdac4 transcripts from zygotic to larval day 5 stage.

Bars indicate numbers of *hdac4* transcripts per million transcripts read at each stage.

Between the 128 and 256-cell stage, maternal transcripts degrade and zygotic transcripts become predominant. See http://www.ebi.ac.uk/gxa/experiments/E-ERAD-475 for Expression Atlas data.

